Research Signpost
37/661 (2), Fort P.O.
Trivandrum-695 023
Kerala, India

Fundamentals and Current Topics in Molecular Structure Research, 2011: 95-113
ISBN: 978-81-308-0458-3 Editors: Prabhakar Misra and Chandran Haridas

4. Simulation and modeling of nanostructures, defects and adsorption processes in materials

D. Casimir, S. Gatica and P. Misra
Department of Physics & Astronomy, Howard University, Washington, DC 20059, USA

1. Introduction

Industrial applications, such as mixture separation, air purification, and surface coatings, all depend on adsorption phenomena. The significant role of interfaces and the need for a better understanding of both physisorption and chemisorption at the microscopic level over the past few decades has motivated the innumerable theoretical developments of the subject. Almost a quarter century ago, carbon research was given a boost by Richard Smalley's discovery of fullerenes and buckyballs [1] and Sumio Iijima's detection of nanotubes [2] - the one-dimensional allotrope of carbon- in the soot of an arc discharge in an effort to synthesize clusters of fullerene. In contrast to buckyballs and nanotubes, which were observed experimentally twenty five years ago, the one-atom-thick sheet of carbon possessing a honey-comb lattice structure called graphene has been an object of theoretical interest for more than fifty years [3]. The awarding of the 2010 Nobel Prize in Physics to Andre Geim and Konstantin Novoselov for the definitive identification and characterization of graphene recognizes a new chapter in carbon research and is testament to the importance of the field [4]. Graphene exhibits the so-called

Correspondence/Reprint request: Dr. P. Misra, Department of Physics & Astronomy, Howard University, Washington DC 20059, USA

Berry phase that determines the material's anomalous quantum Hall effect [5]. Although theoretical implications of this truly two-dimensional material were being worked out more than half a century ago, such as Philip Wallace's mapping of its band structure in 1947 [6] and J.W. McClure's wave equation for excitations in 1956, followed by Hanns-Peter Boehm's experimental synthesis of graphene in 1962 from graphite oxide solution and observation of its fragments via transmission electron microscopy [7], the production of stable mono-layer sheets of carbon was thought to be impossible up until 2004. Earlier in 1994, Boehm had coined the name graphene for the one-atom layered carbon material. In 1999, Rodney Ruoff patterned a graphite surface into the shape of pillars that when rubbed against a silicon wafer created thin multilayer carbon flakes. This approach was improved upon by Philip Kim in 2002, when he synthesized a so-called "nanopencil", as well as graphite flakes that were about ten monolayers thick – about 4 nm. However, a single layer of carbon was not engineered till 2004, when Giem and Novoselov developed a very simple, elegant and economical method for synthesizing good quality graphene [8]. They used Scotch tape to peel away weakly bound layers from a crystal of graphite and subsequently rubbing those layers onto an oxidized silicon surface. Graphene, with its highly regular structure [9], presents the possibility of creating some of the world's most sensitive sensors, where the effects of the adsorption of individual molecules could be exploited.

2. Experimental methods

Over the decades the increased understanding of adsorption phenomena based on measurements using macroscopic thermodynamical methods has been influenced more so by technical and engineering improvements in the processes and apparatuses used, than to refinements of the physical principles that the measurements are based on. Methods primarily based on manometric-volumetric, and calorimetric variants, such as heat capacities, adsorption isotherms, and isosteric heats of adsorption fall in this category. For example, in the late 1960s, the first recorded evidence for sub-monolayer steps in isotherms was given by Thomy and Duval's work (in 1969) as indicated in Ref [10]. This was primarily the result of refinements of temperature control techniques made to the usual volumetric adsorption instruments used at the time. Other capabilities, and unexpected adsorption effects, again due to greater precision in temperature and pressure control, discovered during this period, were isotherms containing extremum values, and being able to correlate specific material properties with the structure and type of adsorption of the adsorbates involved. Somewhat later, W. Langer's

modifications to the volumetric adsorption instruments that existed at that time resulted in the first of what are now known as Sensor Gas Calorimeters (SGC). Transferring the heat flow that normally accompanies the adsorption process to the surrounding gas and then having it flow past the enclosed adsorption chamber; the gas could then be used as a sensor. This process resulted in the ability to measure isotherms, and the heats of adsorption at the same time [10].

Discovered in 1927, by Davisson and Germer, Low Energy Electron Diffraction (LEED) [11], and subsequent diffraction and scattering techniques then took more than 30 years to be implemented as an investigative tool for scientific advances. The onset of electronics that allowed one or more conveniently visualizable diffraction patterns, and other enhancements such as electron channel multipliers that safeguarded against desorption caused by the beam, also made it possible to determine the orientation of adsorbed layers as compared to the adsorbent.

Now with the recognized importance of gas adsorption on nano-scale materials, with applications in the sensing and storage of gases, much has been done in extending our understanding of the role of substrate during film formation [12-16]. Low energy electron diffraction measurements in conjunction with grand canonical Monte Carlo simulations of xenon (Xe) on a single layer of C_{60} molecules on a silver sub-layer, Ag(111), recently performed by Gatica, Li, Trasca, Cole, and Deihl [12] have revealed two distinct steps in the adsorption process. The use of a monolayer of C_{60} molecules on top of a Ag substrate serves well as a stepping block from the extensively studied situation of adsorption involving atomically smooth substrates to more complex situations involving adsorption in porous materials. The first of the two distinct phases of this adsorption process was the xenon adsorbate matching the structural arrangement of the C_{60} monolayer. The LEED investigation of this system began with the preparation of the Ag(111) substrate, which required very high spectroscopic purity in order to reduce the background contribution to the scattering to negligible values. The Ag(111) crystal layer was obtained by the bombardment of a sample with Ar ions. The Ag(111) layered crystal was subsequently diamond polished and chemically etched. The various layers of the C_{60} initially grown through the sublimation of a C_{60} powder sample, were desorbed to obtain a C_{60} monolayer. Based on LEED adsorption isobars of xenon that were collected with a computer operated charge-coupled device camera, two distinct steps on the adsorption curves and three on the desorption curves, were discovered. Compared to the adsorption curve, the steps in the desorption curves were more abrupt than the ones in adsorption isobars, which is usually attributable to adsorption involving nanomaterials

and porous adsorbents. However, this study presented an interesting case where the use of LEED diffraction spots could not be used to sufficiently determine the amount of adsorbate present, in this case xenon. Because the adsorbate xenon was found to only decrease the intensity of the diffraction spots, without introducing any new ones, a disordered layer of adsorbate being formed on the C_{60}/Ag(111) structure was found to be an invalid interpretation of the above-mentioned effects. Therefore, with both the C_{60} and the Ag(111) substrate already contributing to the observed diffraction features, the attenuating effect of the adsorbed xenon more strongly indicates the adsorbate forming a commensurate layer with the C_{60}-Ag(111) adsorbent system. It is this intricate combination of attenuation and diffraction that eliminates the use of scattering intensities in the determination of the amount of xenon adsorbed in this system.

After the replacement of electrons with neutrons, it was then possible to reduce the background contribution to the scattering amplitude to very minimal levels. However, this effect depended on the particular material used for the adsorbent. Scattering with neutrons also allowed larger molecules, such as ammonia and methane to be used as adsorbates, which greatly simplified the determination of adsorbate structure and orientation through scattering techniques due to the high scattering cross-sections of the previously mentioned molecules. The determination of time-dependent properties in addition to structural information is also possible due to the many varieties of neutron scattering. Diffusion coefficients, for example can be obtained through inelastic neutron scattering data. Currently, neutron diffraction is also being applied in the study of quasi one-dimensional phases of adsorbed material on nanotubes and buckyballs. In the case of nanotubes, simulations had predicted single lines of adsorbed atoms to form between the grooves of adjacent carbon nanotubes [16-17], which would then be followed by the creation of a two-dimensional phase with the eventual coverage of the (CNT) with adsorbate [18]. J.V. Pearce et. al. [19] were one of the first to experimentally confirm these predictions, with Helium-4 atoms as the adorbate. Using one of the Carbon nanostructures, known as Single-Walled Carbon Nano-Tubes (SWNT) with closed ends, Pearce's structural measurements of adsorbed Helium-4 in terms of the dosing was able to demonstrate the formation of a 1-dimensional phase at a specific range of coverage values. Neutrons with a wavelength of 2.414 A were directed at the nanotube bundles, with resulting scattering vectors having values between 0.2 and 5.0 A^{-1}. With the spacing between the tubes being approximately 1.4 nm on average, the scattering intensity from SWNT's with Helium-4 adsorbed on them was strictly negative for scattering vectors, Q, smaller than 1.5 A^{-1}. The negative scattering intensities obtained by this authors' study was also

common to similar studies done by other groups using different gas adsorbates. Pearce's study also found this negative intensity to be proportional to the coverage of Helium-4. In contrast, the scattering from bare carbon nano-tubes exhibited one peak at a Q value of approximately 0.55 A^{-1} due to the triangular structure of the SWNT's. Regarding specifically the one dimensional line phase of He-4, this result was confirmed through the positive scattering intensity for scattering vectors, (Q), with values in the intervals, $1.5 < Q < 2.5$ A^{-1} and $3 < Q < 4.5$ A^{-1}.

Spectroscopic methods, especially the more common techniques, such as nuclear magnetic resonance, were employed heavily in the early stages of the controversial debate three decades ago, on the structural ordering of liquid molecules at extremely close distances from solid substrates.

3. Simulation and modeling of defect domains in graphene

Graphene has emerged as an alternative to silicon as a semiconductor material. Its electron mobility is about hundred times that of silicon. Due to the fact that it is both a semiconductor and also possesses good electrical conductivity, graphene is a promising nanomaterial for building miniature electronic devices. Graphene-based transistors have the potential of reaching speeds of about 100 GHz, while at the same time being three times smaller than traditional silicon-based transistors.

An ideal graphene sheet comprises of a honeycomb pattern of six-membered rings. Imperfections in graphene can either occur when it is grown experimentally or defects can be deliberately introduced in the regular honeycomb structure. Defects can be introduced in graphene either via chemical treatment (e.g. exposure to hydrochloric acid) or by bombardment of the material with different kinds of particles (e.g. electrons or ions). Leifer et al. [20] have shown that adding defects to graphene can increase conductivity by as much as an order of magnitude. Atomic-scale defects in graphene layers alter the physical and chemical properties of carbon nanostructures. Both Scanning Tunneling Microscopy (STM) and Transmission Electron Microscopy (TEM) imagery [21] have documented such defects in graphene material sheets. Complex patterns are visible around these defects, which are highly sensitive to the local electronic density of states. Usually, defects act as scattering centers and reduce conductivity in semiconductor materials; however, an increase in the local density of states around defects in graphene serves to add electronic levels at the Fermi energy and therefore significantly enhance its conductivity. As a result, band gaps open up and create regions in which the graphene material behaves as a metal. Batzill and Oleynik et al. [22] have found a novel technique of

extending defects throughout a graphene sheet [23], whereby octagonal and pentagonal carbon rings introduced on idealized graphene sheets behave like quasi-one-dimensional metallic wires with good electrical conductivity.

Density functional theory (DFT) computations serve to elucidate the properties of defects in graphene. A set of stable domain structures have been identified using DFT [24]. For a perfect honeycomb graphene structure, DFT calculations show a zero minimum in the electronic density of states (DOS) at the Fermi level, whereas in the presence of defects or grain boundaries there is a nonzero minimum in the DOS at the Fermi level. Simulation of STM topographic imagery will help to characterize these defect domains in graphene.

4. Nanobubbles

Nanobubbles have been observed to form in solid interfaces. Fig. 1 shows a scheme of a bubble with a shape of a spherical cap. The contact angle is determined based on the solid-liquid-vapor components and temperature.

For a completely non wetting situation, the bubble becomes a flat film of vapor that has zero excess pressure. In the opposite limit of complete wetting, the supported and free bubbles are actually identical.

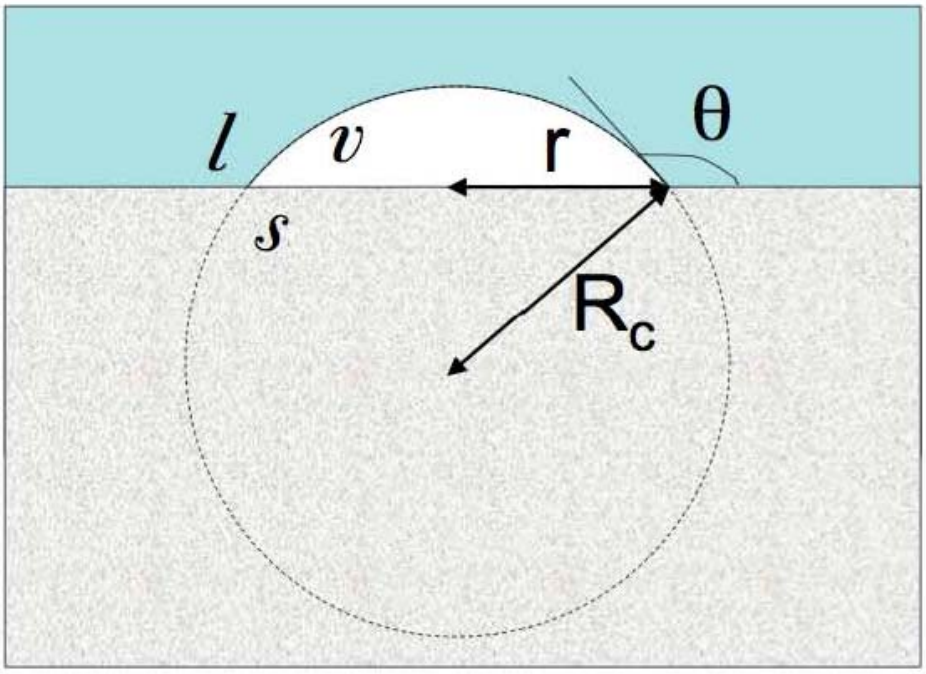

Figure 1. Schematic view of a nanobubble. The light gray curve embedded in the solid represents the virtual sphere that contains the bubble.

Typical size of nanobubbles observed in water-solid interfaces are reported to be as small as r = 150 nm with a contact angle of around 150^o. Our theoretical calculations [25] have shown that the radius of curvature R_c = 300 nm, which yields an excess pressure of ~ 4.7 atm. Such a bubble would require a large amount of energy to form and would be unstable. However, the bubbles are observed to be stable for many hours. Possible explanations for such stability are that the shape is not really spherical, but it has a flat top, and that the surface tension is significantly reduced. In fact, the surface tension does decrease with the radius of curvature for droplets.

Nano-scale bubbles that form on surfaces submerged in some liquids are the cause for much debate. In an effort to explain their experimentally observed long-term stability, one can begin with the Laplace-Young equation in the form:

$$P_i - P_e = 2\sigma/R \tag{1}$$

where P_i is the internal pressure of the bubble, P_e is the external pressure, R is the radius of curvature, and σ is the interfacial surface tension. According to this thermodynamic expression, for radii on the order of nanometers, the internal pressures predicted would be very large causing the bubbles to be unstable and to rapidly diffuse. One possible solution to this problem proposed by Agrawal [26] was to question the applicability of the Laplace-Young Eqn. (1) in its current form to the phenomena of nanobubbles. To justify his argument, he used experimental values for the pressure, volume and temperature of a typical nanobubble, obtained through the use of Atomic Force Microscopy, and then calculated the number of gas molecules inside a nanobubble, by assuming the air inside to obey the ideal gas equation of state:

$$P_{in}V_b = NRT \tag{2}$$

The number of molecules this author calculated for the given experimental values of P, V, and T, was approximately 20 molecules. He next calculated the mean free path, which is the distance traveled by a particle before it collides with another one, using the expression:

$$\lambda = 1/\{\sqrt{(2)}\pi(d^2)n\} \tag{3}$$

where d is the diameter of an air molecule, n is the number of molecules per unit volume, and λ is the mean free path. Again, using his experimental

values the calculated mean free path was 20-30 nm. Therefore, using the fact that the calculated mean free path has dimensions of order of the nanobubble itself, it was concluded that the macroscopic definition of pressure does not apply to the phenomena of nanobubbles. The dimensions of interest need to be much larger than the square of the mean free path in order for pressure to be a continuous macroscopic property.

Our numerical investigation of the stability of surface nanobubbles examined the effects of the adsorption potential strength and temperature of the bulk fluid (water in this instance), on bubble shape, and stability, based primarily on the contact angle. Through a modification of the Young's equation by using the approximation to the solid-liquid interfacial tension, the dependence of the contact angle on the bulk water temperature, and adsorbate potential strength has been computed [27]. The functional form of the potential used in the study neglects the corrugation of the substrate and is given by

$$V(z) = [\{4\ C^3/(27\ D^2 z^9)\} - \{C/z^3\}] \quad (4)$$

What this initial study has shown is that for the case of potential parameters C and D corresponding to graphite, at a temperature of approximately 500 K, there is a wetting transition, where water partially wets the surface for lower temperatures (< 500 K), and completely wets the surface for higher temperatures (> 500 K).

5. Simulations of physical adsorption in carbon nanotubes

Physical adsorption (physisorption) of molecules in carbon nanotubes has been extensively studied by Grand Canonical Monte Carlo simulations [28-32]. When a substrate is exposed to a vapor, physisorption occurs at a vapor pressure higher than the pressure of uptake, P_u, and below saturated vapor pressure (SVP). The value of P_u depends on the strength of the force of the substrate and the temperature of the system. If after having adsorbed molecules from the vapor, the temperature is increased, the molecules are "desorbed".

The accuracy of the computer simulations depends on the model of the potential interaction used. In most cases, carbon nanotubes are typically modeled as smooth cylinders made of carbon with the same areal density of grapheme [33]. This so-called "continuous approximation" provides an accurate description of the adsorption process; however, it fails in describing commensurate phases of the adsorbates [34]. The continuous approximation is usually adopted to save computing time and may be justified by the lack of

information about the chirality of the nanotubes forming a bundle. In the case where an atomistic model is desired, for example if details of the structure of the adsorbed layers are relevant, the nanotube- adsorbate interaction is modeled as a pair wise sum of carbon-adsorbate interactions, $V_{c\text{-}a}$. The potential $V_{c\text{-}a}$ is usually approximated by a Lennard-Jones potential. However, it has recently been shown that, as happens for the interaction with graphite, the anisotropic effects are not negligible and must be included in the force to simulate the formation of commensurate solid layers [35]. The anisotropy is a consequence of the geometry of the substrate that causes the in-plane polarizability of carbon atoms to be higher than the surface-normal polarizability [36].

Another interesting effect worth mentioning here is that of the compression or expansion of the substrate produced by the force of the adsorbate. Although this effect has been observed experimentally and computationally, an overwhelming majority of the theoretical studies have assumed that the environment provides a fixed static potential in which the adsorbate moves. In recent papers [37-38] it was shown that the relaxation of the substrate is not limited to affecting the capacity of the uptake, but has dramatic consequences on the physical properties of the adsorbates, like phase transitions and the energetics in low dimensions. For example, ^{3}He in a rigid 1D pore is a gas, whereas in a non-rigid carbon nanotube it is a liquid.

Figure 2 exhibits the various adsorption sites accessible, in principle, to an adsorbate in a bundle of carbon nanotubes. The external surface region includes the so-called groove between pairs of nanotubes, an energetically favorable site because of the high coordination number of C atoms. Between a triad of nanotubes within the bundle lie “interstitial channels” (ICs) that may be accessible to small atoms or molecules if not blocked at the end. Finally, there exists the “endohedral” region inside the individual tubes; access to this region usually requires chemical treatment to open the tube. Here we summarize the main aspects of endohedral and exohedral adsorption.

Endohedral adsorption of a molecule strongly depends on the radius (R) of the nanotube and the “size” of the molecule. As a result of the analysis of the potential interaction between the adsorbate and the nanotube, it can be seen that adsorption is possible for values of R higher than 0.9σ (where σ is the LJ parameter of the adsorbate). For $0.9\ \sigma < R < 1.212\ \sigma$, adsorption is restricted to the axis of the nanotube, and for $R > 1.212\ \sigma$, the adsorbate forms a cylindrical shell [33]. For wider tubes, an axial line appears surrounded by a cylindrical shell, mimicking the formation of layers on a flat surface. These predictions have been confirmed by computer simulations [39, 28]. Typical values of σ are, for example, 0.256 nm, 0.305 nm, 0.34 nm, 0.345 nm for He, H_2, Ar and CH_4, respectively.

Exohedral adsorption, opposite to endohedral, is possible for all adsorbates regardless of size. The binding energy in the grooves is typically a factor 1.7 times as large as that on graphite. Adsorption starts in the grooves at the uptake pressure. If the pressure of the vapor is increased, keeping the temperature constant, the adsorbate will form a monolayer that includes the atoms in the groove, and eventually a second layer or multilayers before SVP.

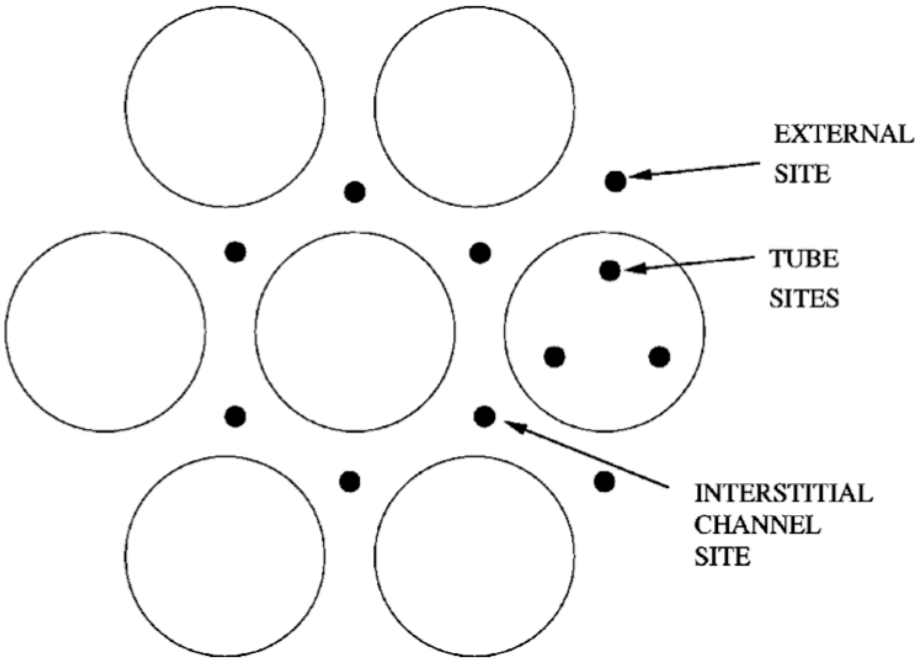

Figure 2. Schematic picture of the adsorption sites in a bundle of carbon nanotubes [Adapted from Ref. 32].

6. Numerical modeling and simulation of nanobubbles and adsorbates on hydrophobic material substrates

Tapping mode Atomic Force Microscopy (AFM) of hydrophobic material surfaces in water shows that they are covered with closely spaced soft domains. The radii of curvature of these features are of the order of 100 nm and their heights above the substrate are in the range 20-30 nm. The consensus in the interpretation of these features is that they are nanosized gas bubbles that are formed on the substrate after immersion. However, there still remains the difficulty of explaining their apparent stability with conventional thermodynamics. Particularly the fact that they are expected to rapidly dissolve because of their high predicted internal pressure. We will present our preliminary results relating to a numerical model of nanobubble/adsorbate

formation on hydrophobic material substrates, which is based on an established approximation of the solid-liquid interfacial tension. Since the predicted number of molecules inside a nanobubble is small (~1000), we have investigated this phenomenon using Molecular Dynamics (MD) simulation [40-42]. The tool of choice has been the classical MD software, namely Large-scale Atomic/Molecular Massively Parallel Simulator (LAMMPS) [41], which has helped provide significant extension to our earlier model. In addition to the interaction between the substrate and adsorbate molecules, by using LAMMPS, one is able to take into account long-range Coulomb forces and utilize the Ewald and/or Particle-Particle-Particle-Mesh (PPPM) methods. Various Lennard-Jones potential parameters associated with the oxygen and hydrogen atoms can be used to run the TIP3P, TIP4P, and SPC models of the rigid water molecules. Dynamic and static properties of water molecules, such as density profiles, pair correlation functions, and velocity auto-correlation functions can be calculated from data produced by MD simulations. Therefore, MD as a tool is well-suited to investigate mechanisms of adsorbate stability on hydrophobic material substrates.

Extending the previously discussed study through the use of molecular dynamics simulation offers a greater level of detail. As mentioned in the introduction, the molecular structure of the substrate and the water molecules can be included through various models of the water-water and water-substrate potential. Interactions between the water and substrate other than Van der Waals interactions can also be explicitly accounted for. However, a significant advantage of molecular dynamics simulation is that due to the deterministic nature of the technique, it will be possible to study the kinetic properties of the system.

The large number of choices of both rigid and flexible water molecule models presents the challenge of choosing the water model(s) best suited to our investigation while providing the most valid and realistic model of the substrate liquid systems under study. As rigid molecular structures with fewer internal degrees of freedom would greatly reduce the required computation, these are the classes of water-molecule models, initially being looked at. Presently we are at the stage of examining the two most commonly used rigid water models shown in Fig. 3., the TIP3P and TIP4P models [40].

In both of these models of water molecules, charges are placed at the locations of the Hydrogen, and Oxygen atoms, commonly called sites, and in the case of the 4-point model (TIP4P), the negative charge is located at a massless site placed along the bi-sector of the HOH angle. The placement and

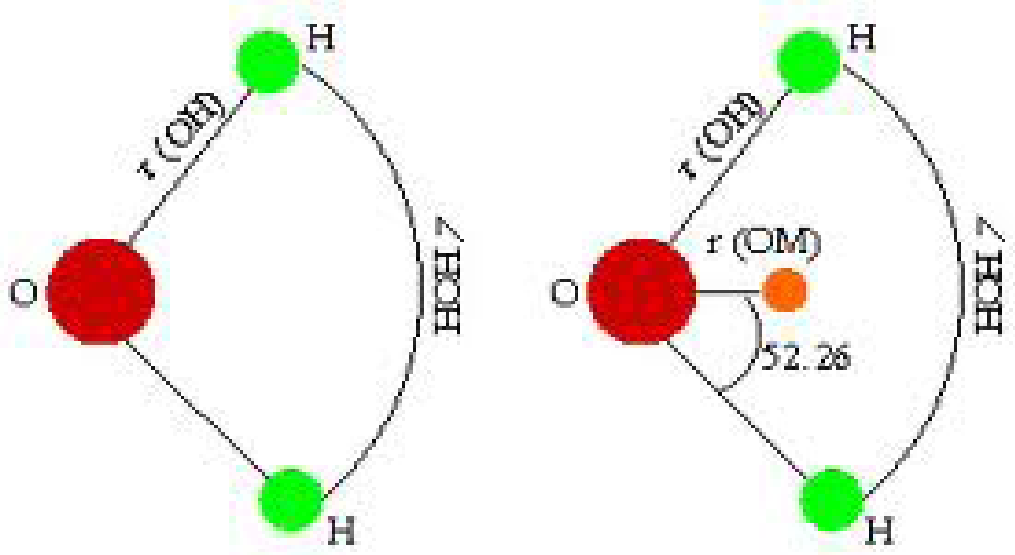

Figure 3. TIP3P Planar Water Model (Left) and TIP4P Water Model (Right).

magnitude of the charges are aimed at modeling the multi-pole moment and other known properties of water. The resulting Coulombic term in the pair-wise additive interaction between all pairs of water model sites, in addition to the Lennard-Jones interactions between the Oxygen sites, allows for the refinement of the previous study's results, based solely on macroscopically looking at Lennard-Jones interactions between substrate and water.

Table 1. TIP3P & TIP4P Parameters [http://lammps.sandia.gov/] Units: mass = grams/mole, distance = Angstroms, energy = Kcal/mole charge = multiple of electron charge (+1.0 is a proton).

TIP4P Parameters	**TIP3P Parameters**
O mass = 15.9994	**O mass = 15.9994**
H mass = 1.008	**H mass = 1.008**
O charge = -1.0484	**O charge = -0.830**
H charge = 0.5242	**H charge = 0.415**
r0 of OH bond = 0.9572	**LJ epsilon of OO = 0.102**
theta of HOH angle = 104.52	**LJ sigma of OO = 3.188**
OM distance = 0.1250	**LJ epsilon = 0.0**
LJ epsilon of O-O = 0.16275	**Sigma of OH, HH = 0.0**
LJ sigma of O-O = 3.16435	**K of OH bond = 450**
LJ epsilon = 0.0	**r0 of OH bond = 0.9572**
Sigma of OH, HH = 0.0	**K of HOH angle = 55**
	theta of HOH angle = 104.52

As shown in Table 1 above, the 3-point model (TIP3P) has an OH bond length of 0.9572 Angstroms, a rigid angle of 104.52 Degrees, and charges of -0.834e, and 0.417e at the Oxygen and Hydrogen sites respectively, in units of the fundamental charge. For the 4-point model (TIP4P) the distance between the Oxygen and mass-less site, M is 0.125 Angstroms, and the charges in units of e, placed at the M and Hydrogen sites respectively, are -1.0484, and 0.5242. The effectiveness of these two models in reproducing the various properties of water is discussed extensively in Refs. [42-45]. Currently, only a few pre-production runs of TIP4P bulk water without any interacting substrates that will need to be equilibrated for a substantial amount of time have been produced. The pair-wise interaction used in those simulations is given by Eqn. (5):

$$V_{ij} = 4\,\varepsilon[\,(\sigma r_{ij})^{12} - (\sigma r_{ij})^{6}] + [Cq_iq_j/(\kappa r_{ij})] \qquad (5)$$

where the first factor involving the square brackets is the usual 6-12 Lennard-Jones interaction, and the second term is the Coulomb potential. The factor C is an energy conversion constant specific to the molecular dynamics simulation program LAMMPS [41] and κ is the dielectric constant of water.

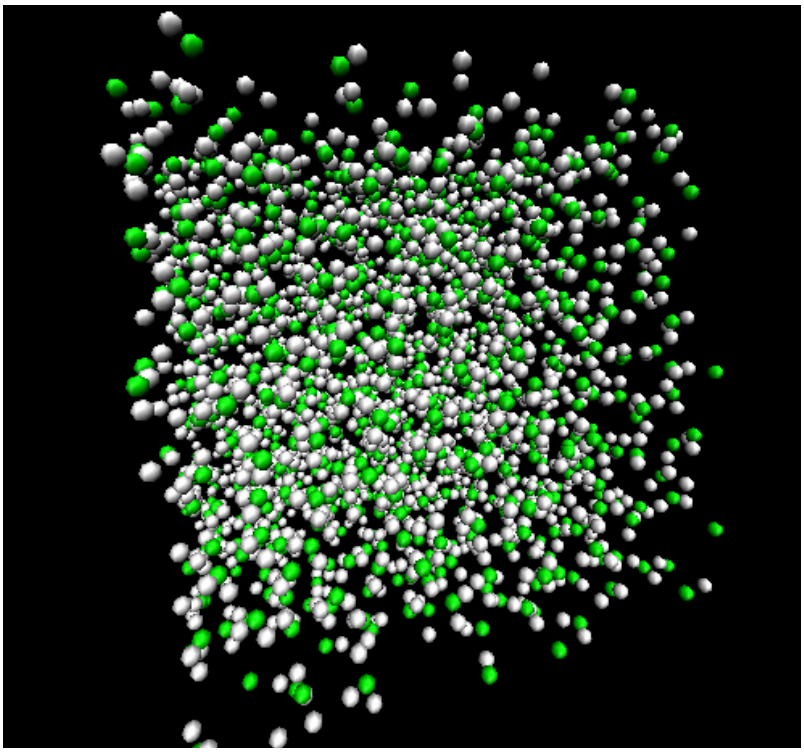

Figure 4. Snapshot of simulation of TIP4P water (Oxygen represented by green, bonds not shown explicitly), 2 picoseconds in duration. The Canonical ensemble (Constant NVT) was used.

The dimensions of the cubic simulation domain are 31.1 x 37.1 x 37.1 Angstroms.

Fig. 4. is an illustration showing a snapshot of the simulation of the TIP4P water model employing the canonical ensemble.

Nanobubbles have the potential for many applications such as the bio-imaging of cells. Understanding the interplay between surface hydrophobicity and adsorbates also has implications for the fabrication and characterization of optical materials. Homogeneous and detailed substrates can be used in conjunction with MD investigations to test a leading hypothesis of solution super-saturation playing a role in nanobubble stability.

7. Nanobubbles on graphene

It has been shown experimentally by Levy et al. [46] that when graphene is stretched to form nanobubbles on a platinum substrate, electrons behave as if they were subject to magnetic fields in excess of 300 Tesla, even though no magnetic field has actually been applied. This is a completely new physical effect that has no counterpart in any other condensed matter system. Levy et al's discovery is significant because for over a century people have been inserting materials into magnetic fields to see how the electrons behave, but it is next to impossible to sustain tremendously strong magnetic fields in a laboratory setting. The current record is 85 Tesla for a field that lasts only of the order of milliseconds. When stronger fields are created, the magnets get destroyed. The ability to make electrons behave as if they were in magnetic fields of 300 Tesla or more – merely by stretching graphene – offers a new approach for important applications and fundamentally new scientific discoveries. It is graphene's unique electronic behavior that makes this potentially feasible.

8. Conclusion

If forced to choose a primary reason for the numerous studies of adsorbed films on various substrates, an argument can be made that it was the growth in the realization among researchers that the adsorbate-adsorbate, and adsorbate-substrate interactions are not mutually exclusive [47]. Evidence showing that adsorbate characteristics are also based on some subtle combination of the two above-mentioned interactions has been actively sought for over two decades now [47]. The survey of the progression of experimental methods and the consequent revelations of adsorbate structure and behavior in Section 2 highlights the above interactions. In addition to adsorption apparatus modifications, such as the first use of electro-pneumatic

valves enabling one to produce automated adsorption and desorption isotherms, it has also long since been established that the conventional cleaning process for the often exfoliated graphite substrate, namely vacuum heating to approximately 900 ^{o}C, is not always sufficient for other substrates, e.g. boron-nitride [47].

With the recent discovery and subsequent rapid increase in the popularity of graphene in materials science, new avenues into the study of low-dimensional physics have opened up [48]. Oddly enough, although graphene is the basis material of buckyballs and carbon nanotubes, it was the latter structural variants of graphene to be used in the initial discovery of the one-dimensional phase of matter that comprised of various adsorbed gas molecules along the grooves and interstitial channels of two and three carbon nanotubes, respectively. The predictions and implications of this realm of physics open to investigation are too numerous to list. Just looking at the transport rates along the interior axes of defect-free nanotubes, which are predicted to be much larger than that of the same gas molecules in zeolites, is responsible for numerous studies thus far [49]. In the case of pure flat graphene sheets, the predictions and discoveries are more surprising. With its unique band structure, charge carriers in graphene are found to obey the Dirac equation, not Schroedinger's, essentially behaving as massless Dirac fermions very near the speed of light [48]. The invaluable property of graphene regarding adsorption however is its much more noticeable reactions to certain chemical changes, which are usually diminished due to bulk effects in other materials. Sensors capable of detecting the amount of gas molecules on the order unity are already in the demonstration stage [50].

Adsorbed water layers - called adlayers – on solid surfaces are very delicate and dynamic under room temperature conditions; and therefore determining their microscopic structure under good resolution is quite a challenge. A recent study [51] by James Heath's group at the California Institute of Technology has documented the presence of trapped water adlayers under a graphene sheet using Atomic Force Microscopy. At room temperature, the first adlayer is in the form of atomically flat islands about tens of nanometers across, with facets angled at 120 degrees, and each island has a height of 0.37 nm - akin to an individual bilayer of crystalline ice. Interestingly, at increased humidity levels, droplets are observed to form on the solid surface.

Defect-ridden graphene sheets are stronger than defect-free graphene sheets. A recent computational study by Grantab et al. [52] shows that graphene sheets with highly misaligned boundaries are stronger than slightly misaligned ones. Misaligned grain boundaries investigated comprised of repeating pairs of 5- and 7-member rings separated by hexagonal rings.

Stress-strain curves were simulated as a function of misalignment, and showed that tensile strength was enhanced as the misalignment angle increased. One of many interesting properties of graphene is its tensile strength of about 100-Gpa, which is roughly 40 times greater than the corresponding value for steel. Thus, looking ahead, it might be more efficient to manufacture graphene sheets with controlled defects than to make defect-free or pristine ones.

The remarkable properties of graphene will help usher in a diverse array of future technologies and applications, ranging from solar panels and transparent touch screens to ultra-strong composite materials and the wondrous so-called "space elevator". One can take a continuously produced sheet of graphene and slice it into thin strips to produce a strong rope. The thin strip formed can be shaped into a slowly twisting tube, which can be wound around other similar ones, to give rise to a very strong rope that would provide a continuous fiber link from ground to a geostationary location and result in a "space elevator". As graphene conducts electrons better than silicon, it can be used to make low-power transistors and ultrafast microprocessors. Thus, computers would be made faster by developing microprocessors that use graphene transistors. In addition, because of graphene's mechanical strength and stretchability, it has the potential of being shaped into a durable, mechanically operated electrical switch for communication devices that would include advanced radar and cell phones. The technological promises of "wondrous" graphene appear to be myriad as the second decade of the twenty first century unfolds.

References

1. "C_{60}: Buckminsterfullerene," H.W. Kroto, J.R. Heath, S.C. O'Brien, R.F. Curl and R.E. Smalley, Nature **318,** 162-163 (1985); doi: 10.1038/318162a0.
2. "Helical microtubules of graphitic carbon," S. Iijima, Nature **354,** 56-58 (1991).
3. "Nobel physics prize honors achievements in graphene," M. Wilson, Physics Today, December 2010, pp. 14-17.
4. http://nobelprize.org/nobel_prizes/physics/laureates/2010/press.html
5. "Experimental Observation of Quantum Hall Effect and Berry's Phase in Graphene," Y. Zhang, Y.-W. Tan, H.L. Stormer and P. Kim, http://arxiv.org/ftp/cond-mat/papers/0509/0509355.pdf
6. "The Band Theory of Graphite," P.R. Wallace, Phys. Rev. **71,** 622-634 (1947).
7. "Graphene and Graphene Oxide: Synthesis, Properties, and Applications," Y. Zhu et al., Adv. Mater. **22,** 3906-3924 (2010); doi: 10.1002/adma.201001068.
8. "Electric Field Effect in Atomically Thin Carbon Films," K.S. Novoselov et al., Science **306,** 666-669 (2004); doi: 10.1126/science.1102896.
9. "Graphene: Status and Prospects," A.K. Geim, Science **324,** 1530-1534 (2009); doi: 10.1126/science.1158877.

10. "Gas Adsorption Equilibria: Experimental Methods and Adsorption Isotherms," J. Keller and R. Staudt, Springer Science & Business Media, Inc., 2005.
11. "Diffraction of Electrons by a Crystal of Nickel," C. Davisson and L.H. Germer, Phys. Rev. **30,** 705-740 (1927).
12. "Xe adsorption on a C60 monolayer on Ag(111)," S.M. Gatica, H.I. Li, R.A. Trasca, M.W. Cole and R.D. Diehl, Phys. Rev.B **77,** 045414 (2008); doi: 10.1103/PhysRevB.77.045414.
13. "Wedge wetting by van der Waals fluids.", M. Napiorkowski, W. Koch and S. Dietrich, Phys. Rev.A **45** (8), 5760-5770 (1992).
14. "Discontinuous behavior of liquids between parallel and tiltied plates.", P.Concus and R. Finn, Phys. Fluids **10** (1), 39-43, (1997).
15. "Filling transition for a wedge," K. Rejmer, S. Dietrich and M. Napiorkowski, Phys.Rev.E **60**, 4027-4042 (1999).
16. "Physical Adsorption on Heterogeneous Solids," M. Jaroniec and R. Mady, Elsevier, Amsterdam, 1988.
17. "Computer Simulation and the Statistical Mechanics of Adsorption," D. Nicholson and N.G. Parsonage, Academic Press, New York, 1982.
18. "Review: Novel Physics of Gases Near Carbon Nanotubes and Buckyballs", S. Gatica, Calbi, Diehl and M. Cole, Journal of Low Temperature Physics, Springer (2008).
19. "One-Dimensional and Two-Dimensional Quantum Systems on Carbon Nanotube Bundles," J.V. Pearce, M.A. Adams, O.E. Vilches, M.R. Jonson and H.R. Glyde, Physical Review Letters **95,** 185302-1– 185302-4 (2005).
20. "Conductivity engineering of graphene by defect formation.", K. Leifer et al., Journal of Physics D: Applied Physics, **43** (4), 1-8 (2010). arxiv http://arxiv.org/abs/0905.1346;
21. "Direct evidence for atomic defects in graphene layers," A. Hashimoto, K. Suenaga, A. Gloter, K. Urita and S. Iijima, Nature **430,** 870-873 (2004); doi:10.1038/nature02817.
22. "An extended defect in graphene as a metallic wire.", J. Lahiri, Y. Lin, P. Bozkurt, I. Oleynik and M. Batzill, Nature Nanotechnology **5**, 326-329 (2010).
23. "Nano-Engineering Defect Structures on Graphene," M. Lusk and L. Carr, Physical Review Letters **100**, 175503-1 – 175503-4 (2008).
24. "Atomic-scale imaging of carbon nanofibre growth," S. Helveg et al., Nature **427,** 426-429 (2004); doi: 10.1038/nature02278.
25. "Formation and Stability of Nanobubbles on Hydrophobic Material Substrates," D. Casimir, S. Gatica and P. Misra. International Conference on Computational & Experimental Engineering and Sciences Conference 2010 (ICCES '10), March 28-April 1, Las Vegas.
26. "An experimental study of nanobubbles on hydrophobic surfaces," A. Agrawal, Master's Thesis, Massachusetts Institute of Technology, 2005.
27. "Nanobubbles at Water-Solid Interfaces: Calculation of the Contact Angle Based on a Simple Model," H. Elnaiem, D. Casimir, P. Misra, S. M. Gatica, Computers, Materials & Continua **368**, 1-12 (2009).
28. "Adsorbed gases in bundles of carbon nanotubes: theory and simulation," M. Mercedes Calbi, Milton W. Cole, Silvina M. Gatica, Mary J. Bojan and J. Karl

Johnson, Chapter 9 of Adsorption by Carbons, edited by E. J. Bottani and J.M. D. Tascón, Elsevier Science Publishing, pp. 187-210, 2008.
29. "Phases of neon, xenon and methane adsorbed on nanotube bundles," M. M. Calbi, S. M. Gatica, M. J. Bojan and M. W. Cole, J. Chem. Phys. **115,** 9975 (2001).
30. "Condensed phases of gases inside nanotube bundles," M. M. Calbi, M. W. Cole, S. M. Gatica, M. J. Bojan and G. Stan, Rev. on Modern Phys. **73,** 857 (2001).
31. "Quasi-one and two-dimensional transitions of gases adsorbed on nanotube bundles," S. M. Gatica, M. J. Bojan, G. Stan and M. W. Cole, J. Chem. Phys. **114,** 3765 (2001).
32. "Uptake of gases in bundles of carbon nanotubes," G. Stan, M. J. Bojan, S. Curtarolo, S. M. Gatica and M. W. Cole, Phys. Rev. B **62,** 2173 (2000).
33. "Low coverage adsorption in cylindrical pores," G. Stan and M.W. Cole, Surf. Sci. **395,** 280-291 (1998).
34. "Solid Phase of Krypton on the Exterior of Individual Single-Walled Carbon Nanotubes," O. Ode and S. Gatica, J. Low Temp. Phys. **161,** 367-374 (2010).
35. "Phase behavior of Ar and Kr films on carbon nanotubes," H-Y. Kim, M. Cole, M. Mbaye and S. Gatica, submitted to J. Phys Chem. A (2011).
36. "Interaction between a He atom and a graphite surface," W. Carlos and M. Cole, Surf. Sci. **91,** 339-357 (1980).
37. "Effects of substrate relaxation on adsorption in pores," H.-Y. Kim, S.M. Gatica, G. Stan and M.W. Cole, J. Low Temp. Phys. **156,** 1–8 (2009); doi: 10.1007/s10909-009-9884-0.
38. "Condensation of Fluids Confined in Non-Rigid Nanopores: With a Little Help from the Substrate," S. M. Gatica and H.-Y. Kim, J. Low Temp. Phys. **157,** 382–394 (2009); doi: 10.1007/s10909-009-9898-7.
39. "Axial phase of quantum fluids in nanotubes," S. M. Gatica, G. Stan, M. M. Calbi, J. K. Johnson and M. W. Cole, J. Low Temp. Phys. **120,** 337 (2000).
40. Google Images: *http://www.google.com/images?q=tip3p&rls=com.microsoft:en-us:IESearchBox&oe=&rlz=1I7RNTNen&um=1&ie=UTF8&source=og&sa=N&hl=en&tab =wi&biw= 1345&bih=446*.
41. http://lammps.sandia.gov/.
42. "The Art of Molecular Dynamics Simulation," D. C. Rapaport, Chapter 8, Cambridge University Press, 2004.
43. W. Jorgensen, "Revised TIPS for Simulation of Liquid Water and Aqueous Solutions," Journal of Chemical Physics **7 (77),** 4156-4163 (1982).
44. "VMD-Visual Molecular Dynamics", W. Humphrey, A. Dalke and K. Schulten, J. Molec. Graphics **14,** 33-38 (1996).
45. "Silica Nanobubbles Containing an Organic Dye in a Multilayered Organic/Inorganic Heterostructure with Enhanced Luminescence," M. Lal, L. Levy, K. S. Kim, G. S. He, X. Wang, Y. H. Min, S. Pakatchi and P. N. Prasad, Chem. Mater. **12,** 2632-2639 (2000).
46. "Strain-induced pseudo-magnetic fields greater than 300 tesla in graphene nanobubbles," N. Levy, S.A. Burke, K.L. Meaker, M. Panlasigui, A. Zettl, F. Guinea, A.H. Castro Neto, and M.F. Crommie, Science **329** (5991), 544-547 (2010).

47. "Adsorption Studies on Boron Nitride Substrates," P. Shrestha, M.T. Alkhafaji, M.M. Lukowitz and G.Yang, Langmuir **10,** 3244-3249 (1994).
48. "The Rise of Graphene," A.K. Geim and K.S. Novoselov, Nature Materials **6,** 183-191 (2007).
49. "Adsorption of Helium and other Gases to Carbon Nanotubes and Nanotube Bundles," R.B. Hallock and Y.H. Kahng, J. Low Temp. Phys. **134** (12), 21-30 (2004).
50. "Graphene: Status and Prospects," A.K. Geim, Science **324,** 1530-1534 (2009).
51. "Graphene Visualizes the First Water Adlayers on Mica at Ambient Conditions," K. Xu, P. Cao and J.R. Heath, Science **329,** 1188-1191 (2010); doi: 10.1126/science.1192907.
52. "Anomalous Strength Characteristics of Tilt Grain Boundaries in Graphene," R. Grantab, V.B. Shenoy and R.S. Ruoff, Science **330,** 946-948 (2010); doi: 10.1126/science.1196893.